Applied Surface Science Advances 24 (2024) 100657

Contents lists available at ScienceDirect

Applied Surface Science Advances

journal homepage: www.sciencedirect.com/journal/applied-surface-science-advances

Full Length Article

The formation of calcium glycerolate as an active species in the synthesis of biodiesel. A DFT study

A.J.González Fá [a], P. Bechthold [a], A. Juan [a], J.M. Marchetti [b,*]

[a] Instituto de Física del Sur (IFISUR), Departamento de Física, Universidad Nacional del Sur (UNS), CONICET, Av. L. N. Alem 1253, B8000CPB Bahía Blanca, Argentina

[b] Faculty of Science and Technology, Norwegian University of Life Sciences, Drøbakveien 31, 1432 Ås, Norway

ARTICLE INFO

Keywords:
Glycerol
DFT
Adsorption
CaO
Biodiesel

ABSTRACT

Numerous studies have reported that the addition of glycerol at the onset of an oil transesterification reaction with methanol, catalyzed by CaO, significantly accelerates the reaction. The role of glycerol, which is also a reaction product, is not yet fully understood. The formation of glycerolate structures, in both solid and polymeric forms, has been proposed to actively contribute to the reaction rate. In previous works, we have simulated the formation of incipient OH and ethoxide species on the CaO during ethanol adsorption, and bidentate species between formic acid and the surface. In the present work we have investigated, using DFT-based simulations, the possible initial stages in the formation of glycerolate on CaO (001) surfaces. Our results indicate the bonding of two OHs from glycerol with the surface. We also detected the possible rupture of these OHs by a strong decrease in the bonding order (BO), up to 75%. At the same time, the formation of $O_{glycerol}$–Ca bonds and the decrease in the BO of the surface Ca–O bonds of up to 61% are detected. A charge transfer from the surface to the molecule is also observed. Additionally, a detailed analysis of the changes in the geometry and electronic structure of the glycerol and the surface before and after adsorption is conducted.

1. Introduction

Traditional fossil fuels represent the predominant global energy source extensively employed in industrial processes, electricity production, and transportation around the world. Nevertheless, these resources are non-renewable, experience rapid depletion, and are responsible for greenhouse gas emissions, global warming, and acid rain, among other negative environmental impacts. There are several options to mitigate these issues, and among them, biodiesel stands out as a primary candidate, offering an alternative to traditional diesel derived from fossil sources [1,2]. This biofuel offers advantages like lower CO_2 production, high combustion efficiency, inherent lubricity, biodegradability, and reduced sulfur content [1,2]. Biodiesel can be described as long-chain fatty acid methyl esters (FAMEs) obtained from vegetable oils or animal fats through a transesterification reaction, with glycerol produced as a byproduct [3]. However, the production of high-purity biodiesel at a low cost still presents significant challenges for the scientific community and manufacturers [4]. For example, using conventional edible oils as feedstock may increase prices and trigger a 'food vs. fuel' debate. As a response, various alternatives have been proposed, including non-edible food crops, waste cooking oil, as well as algae and microorganisms. [1,5].

Regarding the transesterification process, in the absence of catalysts, high pressures, elevated temperatures, and extended reaction times, as well as complex glycerol recovery procedures, are essential factors. These elements contribute significantly to the overall cost, rendering the process impractical for large-scale manufacturing [1,6]. In order to avoid these issues, various catalysts are commonly employed in biodiesel production to accelerate the process and enhance the final product yield. Consequently, several catalysts are commonly employed in biodiesel production to accelerate the process and enhance the final product yield. Likewise, it is important to highlight that an appropriate catalyst must possess selectivity, stability, cost-effectiveness, and reusability [7]. These agents can be classified into three main groups: homogeneous, heterogeneous, or enzymatic [1,8].

Homogeneous catalysts exist in the same phase as the reactants and are widely used in biodiesel production. These catalysts can be classified into acidic types, such as sulfonic, sulfuric, and hydrochloric acid, or basic types, such as methoxides, sodium hydroxide, and potassium hydroxide, among others [8]. The choice between acidic and basic

* Corresponding author.
E-mail address: Jorge.mario.marchetti@nmbu.no (J.M. Marchetti).

https://doi.org/10.1016/j.apsadv.2024.100657
Received 9 September 2024; Received in revised form 29 October 2024; Accepted 3 November 2024
Available online 11 November 2024
2666-5239/© 2024 The Author(s). Published by Elsevier B.V. This is an open access article under the CC BY license (http://creativecommons.org/licenses/by/4.0/).

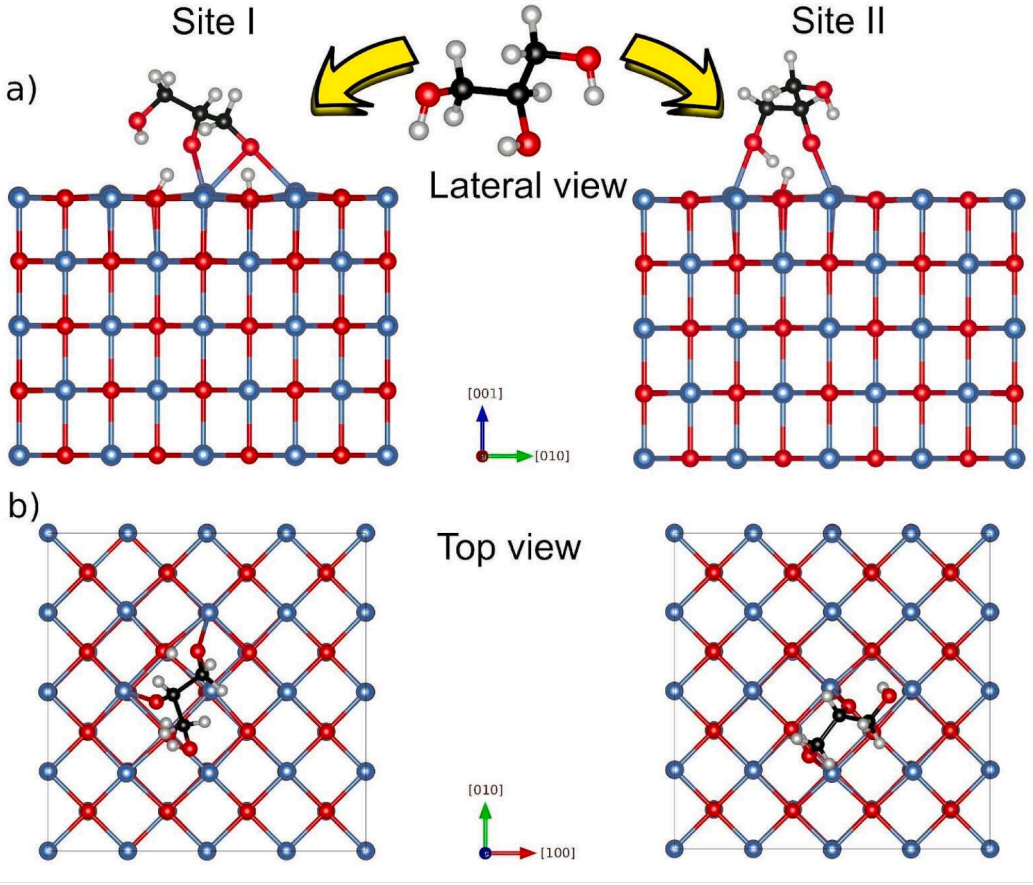

Fig. 1. (a) Lateral and Top view of the two adsorption sites found for glycerol over the CaO (001) surface. Blue, red, black, and gray spheres represent Ca, O, C, and H atoms, respectively.

catalysts mainly depends on the concentration of free fatty acids (FFA) in the raw materials. In this way, homogeneous catalysis in the transesterification reaction presents several drawbacks. For example, acid catalysis is usually slower than basic catalysis, requires elevated temperatures, and, due to the acidic environment, the equipment used in the process must be resistant to corrosion [6,8–10]. On the other hand, basic catalysis usually leads to the formation of soap byproducts when the concentration of FFA is higher than 1% [5,11]. Moreover, both reactions involve hazardous reactants, posing risks to human health, and incur high costs in the purification and separation process [9]. Finally, enzymes prove to be excellent catalysts in transesterification due to their specificity, ability to function at moderate pH, temperatures, and pressures, and the production of high-quality glycerol with minimal waste. However, enzymes as catalysts come with elevated costs, extended reaction times, and high concentration requirements [6,8].

In addressing these challenges, heterogeneous catalysts emerge as an excellent alternative, offering advantages such as reusability, post-reaction recovery, low cost, and environmental friendliness [12–14]. Several heterogeneous catalysts were studied over the years by different researchers, among them, Calcium Oxide (CaO) showed an excellent performance and is the most widely used in the transesterification process [15–17]. Furthermore, CaO possesses a high number of active sites and is cheap and abundant in nature. It can be obtained from various low-cost sources such as eggshells, fish and chicken bones, and clamshells, among others [18]. Concerning the CaO surface, the literature indicates that the (001) face is the most stable [19,20].

As previously mentioned, glycerol is a by-product of the transesterification reaction, and several authors have reported the interaction between this alcohol and the CaO surface. For example, Lopez-Granados et al. [21] have demonstrated that a small amount of glycerol in the initial mixture increases the reaction rate. In their study, the authors concluded that the formation of active surface Ca glyceroxide species is responsible for the improvement in the reaction. Moreover, Kouzu *et al.* [22,23] have identified calcium diglyceroxide (CaD) as a solid catalyst obtained after the biodiesel production process as a consequence of the side reaction in which these compounds (CaO and glycerol) interact or combine. Some studies have even pointed out that the formation of CaD in the initial stages of the reaction promotes the creation of active sites on the surface, enhancing the reaction rate and, consequently, the production of FAMEs [24,25]. However, some researchers have suggested that CaD is less active than CaO and may lead to leaching of calcium from the surface, making it unsuitable for use as a heterogeneous catalyst in the transesterification reaction [26].

In order to achieve a better knowledge of the process, several researchers have studied biodiesel production through Density Functional Theory (DFT) approaches. For example, Li *et al.* employed *ab initio* calculations to explore the role of protons in the mechanism of acid-catalyzed transesterification, finding optimal reaction paths and activation energies [27]. In addition, researchers have explored the behavior of several organic compounds involved in biodiesel production with metal oxide surfaces. For instance, computational methods were employed to investigate the adsorption of ethanol and ethylene glycol on CaO, revealing the formation of energetically favorable systems as a result of the formation of new bonds [20,28]. To deepen our understanding of triglyceride reactions on heterogeneous catalysts, Bechthold *et al.* investigated the interaction of formic acid and ethyl formate with the CaO surface. In the former case, bidentate formate species were observed, establishing bonds with two Ca atoms from the slab. In the latter, ethyl formate developed new bonds between the oxygen and carbon atoms of the molecule and the calcium and oxygen atoms of the

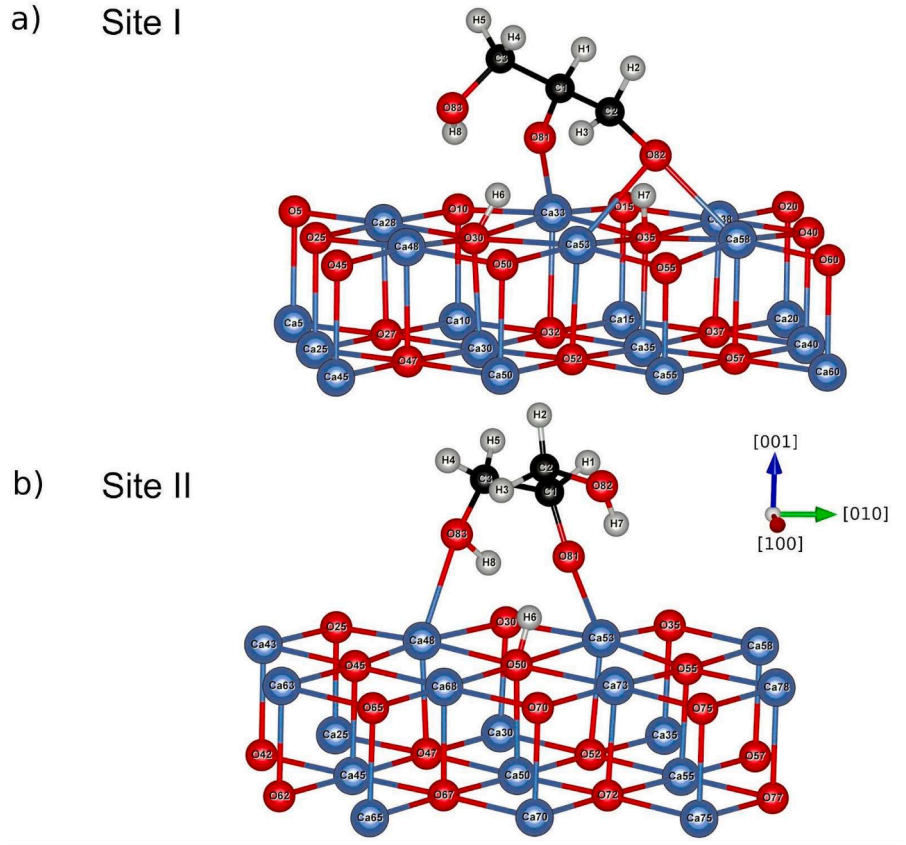

Fig. 2. Magnification of the two adsorption sites found for glycerol adsorption over CaO (001) with the labels utilized in the discussion of the results. Blue, red, black, and gray spheres represent Ca, O, C, and H atoms, respectively.

Table 1
Bond distances, after and before, and the percentage change for glycerol adsorption on site I. For surface atoms, only bond distances varying more than 8% are reported.

Group	Bonded Atoms	Bond Distances (Å)		
		Before	After	Difference %
Glycerol				
	O82–H7	0.98	1.52	55.92
	C2–O82	1.43	1.39	−2.53
	C2–H2	1.10	1.11	0.84
	C2–H3	1.11	1.13	2.30
	C2–C1	1.53	1.56	2.02
	C1–H1	1.10	1.11	0.47
	C1–O81	1.44	1.40	−2.77
	O81–H6	0.98	1.51	54.91
	C1–C3	1.53	1.55	1.72
	C3–H4	1.10	1.10	0.00
	C3–H5	1.10	1.10	0.00
	C3–O83	1.43	1.44	0.56
	O83–H8	0.97	0.99	1.64
Surface				
	Ca33–O30	2.42	2.71	11.79
	Ca53–O30	2.42	2.68	10.59
	Ca53–O35	2.42	2.70	11.48
New Bonds				
	O82–Ca58	–	2.43	–
	O82–Ca53	–	2.51	–
	H7–O35	–	1.03	–
	H6–O30	–	1.03	–
	O81–Ca33	–	2.34	–

Table 2
Bond distances, after and before, and the percentage change for glycerol adsorption on site II. For surface atoms, only bond distances varying more than 8% are reported.

Group	Bonded Atoms	Bond Distances (Å)		
		Before	After	Difference %
Glycerol				
	O82–H7	0.98	0.99	0.91
	C2–O82	1.43	1.43	0.00
	C2–H2	1.10	1.10	0.00
	C2–H3	1.11	1.11	0.00
	C2–C1	1.53	1.54	0.61
	C1–H1	1.10	1.11	0.94
	C1–O81	1.44	1.40	−3.43
	O81–H6	0.98	1.60	63.86
	C1–C3	1.53	1.57	2.74
	C3–H4	1.10	1.10	0.00
	C3–H5	1.10	1.11	0.25
	C3–O83	1.43	1.42	−0.96
	O83–H8	0.97	1.07	10.07
Surface				
	Ca48–O30	2.42	2.63	8.47
	Ca53–O30	2.42	2.72	12.37
New Bonds				
	O83–Ca48	–	2.38	–
	O81–Ca53	–	2.26	–
	H6–O50	–	1.02	–

slab, respectively. Strong adsorption energies were computed in both cases [29,30].

In this study, we investigated the interaction between glycerol and CaO (001) surface. Our goal was to elucidate the role of this polyalcohol in the initial stages of the transesterification process by employing energetic, bonding, and charge transfer analyses. The formation of new species between these compounds is crucial for identifying potential active sites that enhance the rate of methanolysis and catalyze the

Table 3
Bond Order, after, before, and the percentage change for glycerol adsorption on site I.

Group	Bonded Atoms	Bond Order		
		Before	After	Difference %
Glycerol				
	O82–H7	0.8388	0.2357	−71.90
	C2–O82	1.1679	1.3391	14.66
	C2–H2	0.8410	0.8486	0.90
	C2–H3	0.8504	0.8116	−4.56
	C2–C1	0.9134	0.8494	−7.01
	C1–H1	0.7925	0.8116	2.41
	C1–O81	1.0448	1.2055	15.38
	O81–H6	0.8417	0.2421	−71.24
	C1–C3	0.9237	0.8569	−7.23
	C3–H4	0.8436	0.8487	0.60
	C3–H5	0.8634	0.8756	1.41
	C3–O83	1.1426	1.1101	−2.84
	O83–H8	0.8568	0.7862	−8.24
Surface				
	Ca33–O30	0.2760	0.1069	−61.27
	Ca53–O30	0.2764	0.1253	−54.67
New Bonds				
	O82–Ca58	–	0.2094	–
	O82–Ca53	–	0.1371	–
	H7–O35	–	0.7143	–
	H6–O30	–	0.7327	–
	O81–Ca33	–	0.2478	–

Table 4
Bond Order, after, before, and the percentage change for glycerol adsorption on site II.

Group	Bonded Atoms	Bond Order		
		Before	After	Difference %
Glycerol				
	O82–H7	0.8388	0.8190	−2.36
	C2–O82	1.1679	1.1637	−0.36
	C2–H2	0.8410	0.8584	2.07
	C2–H3	0.8504	0.8562	0.68
	C2–C1	0.9134	0.8808	−3.57
	C1–H1	0.7925	0.8085	2.02
	C1–O81	1.0448	1.2260	17.34
	O81–H6	0.8417	0.2091	−75.16
	C1–C3	0.9237	0.8355	−9.55
	C3–H4	0.8436	0.8409	−0.32
	C3–H5	0.8634	0.8706	0.83
	C3–O83	1.1426	1.1715	2.53
	O83–H8	0.8568	0.6475	−24.43
Surface				
	Ca48–O30	0.2761	0.1435	−48.03
	Ca53–O30	0.2764	0.2189	−20.80
New Bonds				
	O83–Ca48	–	0.2097	–
	O81–Ca53	–	0.2959	–
	H6–O50	–	0.7487	–

synthesis of biodiesel.

2. Theoretical methods

We have performed simulations based on density functional theory, implemented through the Vienna Ab-initio Simulation Package (VASP) which solves Kohn-Sham equations considering periodic boundary conditions [31–33]. The core electrons of the elements considered in the simulations were represented by the Bloch's augmented wave approach [34], while the valence electrons were represented by plane waves [35, 36] with a cutoff energy of 550 eV. The pseudopotentials were used with the following valence electrons: Ca ($4s^2$), O ($2s^2\ 2p^4$), C ($2s^2\ 2p^2$) and H ($1s^1$). For the exchange-correlation interactions, we consider the Perdew-Burke-Ernzerhof functional with the generalized gradient approximation. Van der Waals interactions were included through the DFT-D3 method proposed by Grimme [37].

The Brioullin zone was sampled with a (7 × 7 × 1) grid with a Monkhorst-Pack distribution scheme [38]. The simulations were performed until the system reached convergence with a tolerance of 1×10^{-4} eV in energy and 1×10^{-3} eV/Å in force. To simulate the CaO (001) surface, a supercell with 80 Ca and 80 O atoms were considered with a vacuum distance of 30 Å to avoid interactions between the adsorbate and the periodic replications of the surface. Over this supercell we consider the glycerol adsorption at low coverage (≈1/6 ML), mapping all possible adsorption sites and considering different initial approach configurations for the glycerol towards the surface (for more details about the supercell dimensions and the different adsorption sites considered, see Supplementary Material).

The glycerol adsorption energy over the CaO (001) was determined through

$$\Delta E_{ads} = E(CaO + C_3H_8O_3) - E(CaO) - E(C_3H_8O_3) \quad (1)$$

where the first term of the right side of the equation represents the energy (E) of the system with the adsorbate, the second term represents the energy of the clean supercell (without the adsorbate) and the final term is the energy of the glycerol molecule. To obtain the last term, we consider the glycerol molecule inside a 20 Å sides cubic box and perform a gamma point calculation.

After determining the locations of the most favourable adsorption sites, we investigate the characteristics of the bonds with the surface. To this end, we carry out various analyses. We investigate the orbitals participating in the bond through the density of states (DOS) analysis [39]. The net charge of the elements before and after adsorption was investigated according to the Bader technique [40–42] where the bond strength was explored through the bond order (BO) analysis [43–46].

3. Results and discussion

3.1. Glycerol adsorption on CaO (001)

Simulations of the adsorption of glycerol on the CaO (001) surface reveal two possible adsorption sites, as depicted in the lateral and top views of Fig. 1. For a better understanding and more clarity, Fig. 2 shows the corresponding configuration magnifications, including the atom labels. In the two geometries, the bonding with the surface is developed mainly through the interaction between oxygen atoms of the adsorbate with calcium atoms from the surface. The adsorption energies obtained for both sites are very close, being −2.24 eV for Site I and −2.07 eV for Site II, which is consistent with results obtained by Calatayud *et al.* [47]. The similarity in these two values is the reason for performing the following analysis on both configurations.

The effect of glycerol adsorption on the bond distances for the surface and molecule atoms is summarized in Table 1 and Table 2 for sites I and II, respectively.

For the first geometry, we find that the main changes in the distances of the adsorbate occur in the O82–H7 and O81–H6 bonds. After adsorption, these two hydrogen atoms move away from glycerol to form new bonds of 1.03 Å with the O atoms belonging to the surface. The effect of the adsorption process on the rest of the molecule is less significant, with shortenings of 2.53% and 2.77% computed for the C2–O82 and C1–O81 bonds, respectively. Furthermore, new interactions of the molecule with the CaO take place primarily through the O81 and O82 atoms of the alcohol, which interact with three calcium atoms at distances ranging from 2.34 Å to 2.15 Å. Regarding the surface, the adsorption process introduces changes in the adsorbent, producing stretches of up to 11.79% in the Ca − O bonds near the interaction site.

Concerning site II, the adsorption of glycerol mainly occurs through the O83 and O81 atoms of the molecule with two calcium from the oxide forming new Ca − O bonds of 2.26 Å and 2.38 Å respectively (see

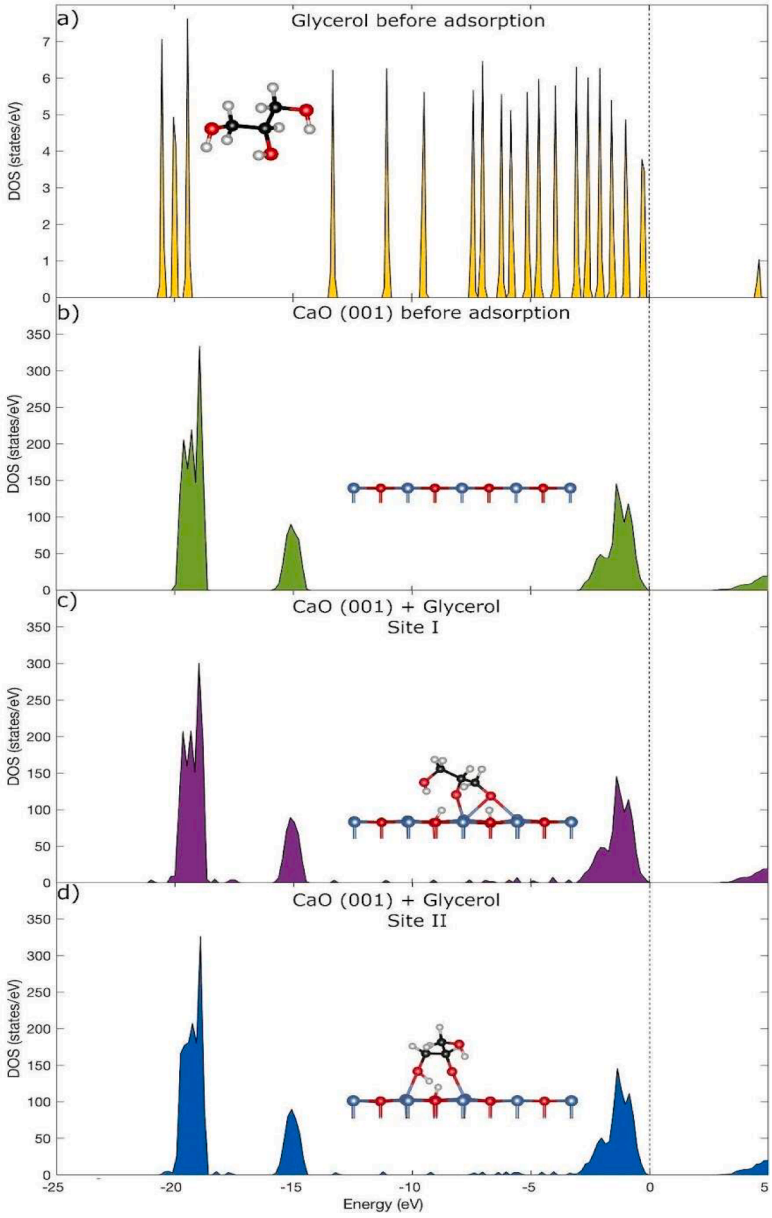

Fig. 3. Total DOS for glycerol and CaO (001) surface before and after the adsorption. The Fermi level is set at 0 eV.

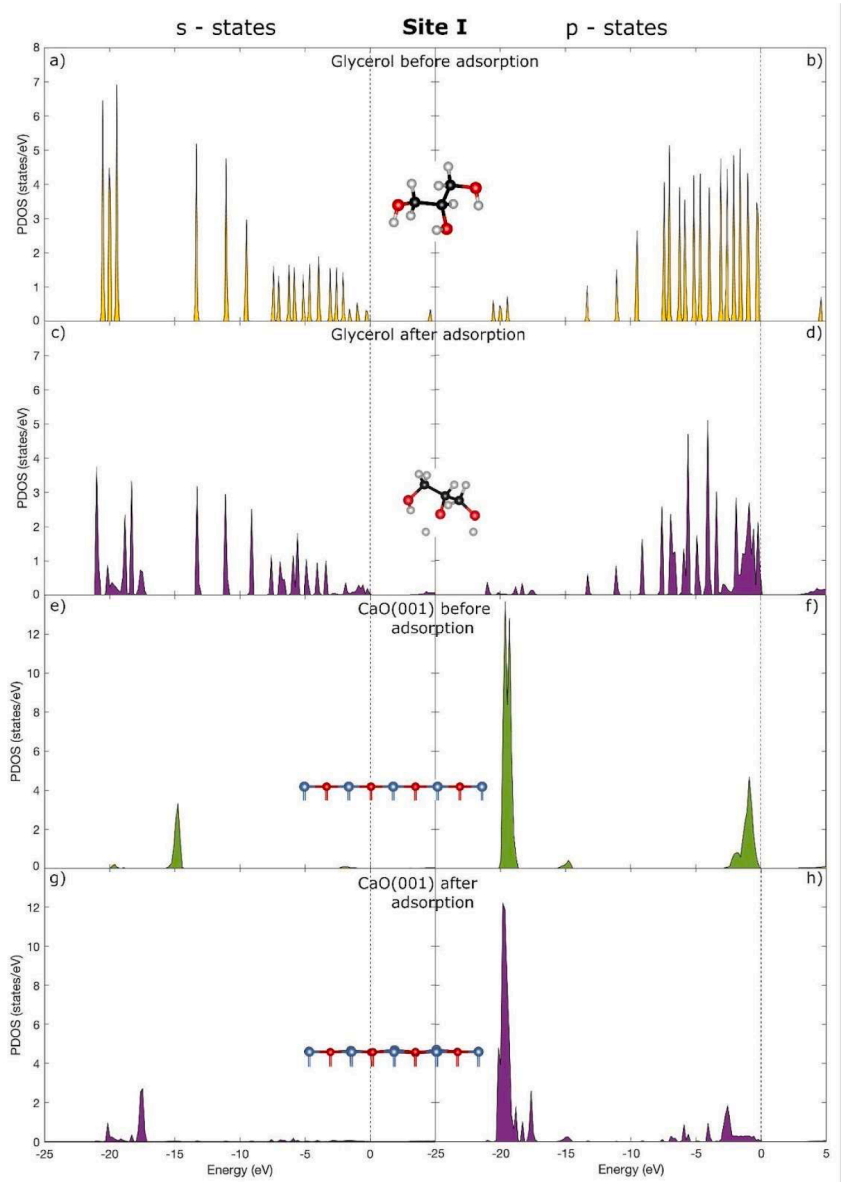

Fig. 4. PDOS onto p and s states for glycerol and the most involved atoms of the surface in the adsorption on Site I (Ca33, Ca53, Ca58, O30 and O35), before and after adsorption. The Fermi level is set at 0 eV.

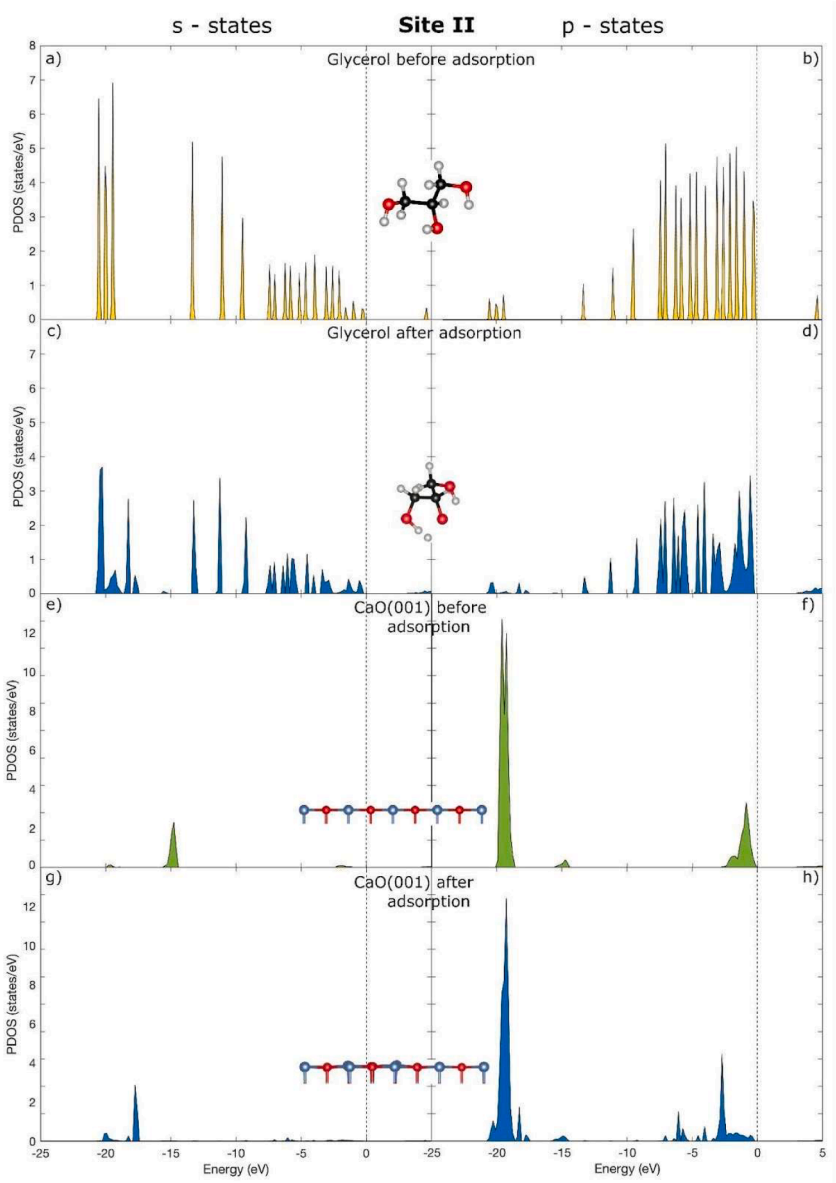

Fig. 5. PDOS onto p and s states for glycerol and the most involved atoms of the surface in the adsorption on Site II (Ca48, Ca53, O50), before and after adsorption. The Fermi level is set at 0 eV.

Table 2). The main change in the molecule is observed for O81–H6, where the H6 atom remains closer to the surface than the rest of the molecule and forms a bond with an oxygen atom of the oxide, with a distance of 1.02 Å. In the alcohol, another remarkable variation is observed in the O83–H8 stretching, which increases by 10.07%. In a similar manner to the previously analyzed configuration, the separation between the atoms near the adsorption site on the surface experiences an elongation, in this case up to 12.37%. It is important to highlight that in none of the obtained configurations do the three oxygen atoms from glycerol interact with the surface simultaneously. These results are in good agreement with previous DFT studies in which glycerol was adsorbed on oxide metal surfaces through two hydroxyl groups [48–51].

Considering that the transesterification reaction is carried out with a methanol/triglyceride ratio greater than 10:1, it is important to think about whether the excess of this alcohol interferes competitively with the adsorption of glycerol on the catalyst surface. According to DFT studies carried out by Li et al. [52,53], methanol preferentially binds via its OH group on a Ca atom from the oxide surface, releasing an H and forming a new Ca—Ometoxy bond. The absorption energy of this process is −1.33 eV, thus representing almost half of the value obtained in the present work for the interaction between glycerol and CaO. According to our calculations, the polyalcohol adsorption is much more stable on the surface when compared to methanol. It is also interesting to mention that Rohmann and Idriss found a similar behaviour for the interaction of oxygenates on rutile TiO2 (110) [51]. These authors report an adsorption energy for methanol of 1.55 eV and 2.68 eV in the case of glycerol. Experimental studies match the preference of this catalyst for glycerol. Kouzu et al. analysed CaO recovered after the transesterification reaction using XDR, IR spectroscopy and 13C-NMR, among other techniques [22,23]. The results revealed the presence of Ca glyceroxide without finding any traces of the Ca-methoxide groups, thus demonstrating that CaO is more reactive to glycerol compared to methanol. Esipovich et al. [54] obtained similar results when they synthesized Ca glyceroxide in the presence of an excess of methanol. Their IR spectroscopy data demonstrated that glycerol displaced methanol from the surface and formed a more stable compound.

Table 5
Bader net charges for Glycerol and most relevant surface atoms corresponding to adsorption on Site I.

Group	Bonded Atoms	Charge (*e*)		
		Before	After	Difference
Glycerol				
	C1	0.44	0.43	−0.01
	C2	0.44	0.43	−0.01
	C3	0.47	0.24	−0.23
	O81	−1.11	−1.14	−0.03
	O82	−1.10	−1.19	−0.08
	O83	−1.14	−0.98	0.16
	H1	0.05	0.02	−0.03
	H2	0.06	0.04	−0.02
	H3	0.04	−0.07	−0.11
	H4	0.06	0.03	−0.02
	H5	0.04	0.02	−0.02
	H6	0.59	0.61	0.02
	H7	0.59	0.63	0.03
	H8	0.59	0.58	−0.01
Surface				
	Ca33	1.49	1.51	0.02
	Ca53	1.49	1.50	0.01
	Ca58	1.49	1.53	0.03
	O30	−1.49	−1.44	0.05
	O35	−1.49	−1.45	0.04

Table 6
Bader net charges for Glycerol and most relevant surface atoms corresponding to adsorption on site II.

Group	Bonded Atoms	Charge (*e*)		
		Before	After	Difference
Glycerol				
	C1	0.44	0.54	0.11
	C2	0.44	0.45	0.01
	C3	0.47	0.44	−0.03
	O81	−1.11	−1.23	−0.12
	O82	−1.10	−1.15	−0.05
	O83	−1.14	−1.22	−0.08
	H1	0.05	−0.01	−0.06
	H2	0.06	0.03	−0.02
	H3	0.04	0.00	−0.04
	H4	0.06	0.03	−0.03
	H5	0.04	0.00	−0.04
	H6	0.59	0.61	0.02
	H7	0.59	0.59	0.00
	H8	0.59	0.61	0.02
Surface				
	Ca48	1.49	1.51	0.02
	Ca53	1.49	1.50	0.01
	O50	−1.49	−1.44	0.05

3.2. Bonding analysis

The strength of the bonds, before and after adsorption, is analyzed by calculating the bond order (BO). The most significant variations in this measure are summarized in Table 3 and Table 4 for Site I and Site II, respectively.

The obtained BO values of the glycerol bonds after adsorption on Site I show a remarkable weakening of 71.24% and 71.90% for the H6–O81 and H7–O82 interactions, respectively. These results indicate that these bonds are broken, which is consistent with the notable elongations reported in Table 1. The other significant BO modification in the alcohol after the geometric relaxation is observed in the C2–O82 bond, with a 14.66% increase. This change aligns well with the distance decrease reported in Table 1, indicating a strengthening in this interaction. Regarding the surface, weakenings of up to 61.27% are reported in the Ca–O bonds near the adsorption site in agreement with the elongation previously reported. Furthermore, the new Ca–$O_{glycerol}$ and Ca–$O_{surface}$ bonds have similar distances and bond order (BO) values, indicating that these new interactions can be considered stable.

On the other hand, for site II, the BO analysis shows a significant decrease in the H6–O81 BO with a variation of −75.16%, consistent with the length increase previously reported, indicating a broken bond. On the other hand, for this configuration, the strength of the O82–H7 bond remains relatively unchanged, while a (BO) change corresponding to H8–O83 is observed with a variation of −24.43%. However, this value, along with the slight increase in bond length, suggests that the bond does not break after adsorption. Regarding the surface, the Ca–O interactions in the vicinity of the adsorption site experience a BO reduction of up to 48%, consistent with the elongations reported in Table 2. This weakening is significant, but less pronounced than that reported for site I. Finally, the new bonds developed after the adsorption process show BO values corresponding to stable interactions.

3.3. Electronic structure and Bader analysis

We have also analyzed the electronic structure of the system in order to determine the orbitals involved in the adsorption process and the characteristics of the new bonds developed. To that end, we have calculated the Density of States (DOS) of the adsorbate and the surface, before and after adsorption. Comparing the total DOS of the CaO (001) surface before adsorption (Fig. 3b), with the system after adsorption (Fig. 3c for Site I and 3d for Site II), we can appreciate the apparition of small states in the range −20 to 0 eV, as a result of the hybridization of CaO states in that range. Due to the low coverage considered in our simulation, in order to appreciate in more detail the orbitals that are being modified on the adsorption process; we have projected the DOS (PDOS) on the most relevant atoms and also on s and p states, for each adsorption configuration. In Fig. 4 we can appreciate the PDOS for Site I. We can observe that the effect of the adsorption on the s-states of glycerol (Fig. 4a-d) is a hybridization of states around −20 eV, while on the p-states we can appreciate an increase of the states near the Fermi level, giving a metallic character to the adsorbed molecule. The latter can also be seen in the s-states but in a more subtle way. For the most relevant atoms of the CaO(001) surface in the glycerol adsorption on Site I (Ca33, Ca53, Ca58, O30 and O35- Fig. 4e-h), we can appreciate a shift of the s-states tho lower energies, indicating a stabilization of such states, while on the p-states we observe greater interaction, with a very well defined hybridization of states, both on the −20 eV zone, as close to the Fermi level. This indicates that the s-states and p-states of the surface are involved in the bonding of the glycerol to the surface. In Fig. 5 we can appreciate the PDOS for site II. For the glycerol molecule (Fig. 5a-d), the interaction with the surface has a similar effect on the atomic states than in the case of Site I, that is to say, a hybridization of s-states around −20 eV, and an increase of p-states around Fermi level. On the other hand, the PDOS for the surface atoms most involved in the adsorption process on Site II (Ca48, Ca53, O50) reveals that also both s and p states participate in the bonding of glycerol to the surface. We can again appreciate a stabilization of the s-states as in the case of the former adsorption site and a hybridization of p-states in the zone of −20 eV and around the Fermi level, being in this configuration slightly more intense than in the case of Site I.

To complete the adsorption characterization, we have also calculated the Bader charges of the system to demonstrate charge transfer between the glycerol and the CaO(001) surface. The results are shown in Table 5 and Table 6 for Site I and Site II, respectively. For both sites, we detected a small electron transfer from the surface to the glycerol molecule. For Site I, the charge transfer is 0.35 *e* from the CaO (001) to the adsorbate, while in the Site II configuration, this value is 0.30 *e*, also from the surface to the adsorbed molecule. In order to have a better visualization of the charge distribution after the adsorption, we show in Fig. 6 the charge density difference (CDD) for both adsorption configurations, calculated using the following equation:

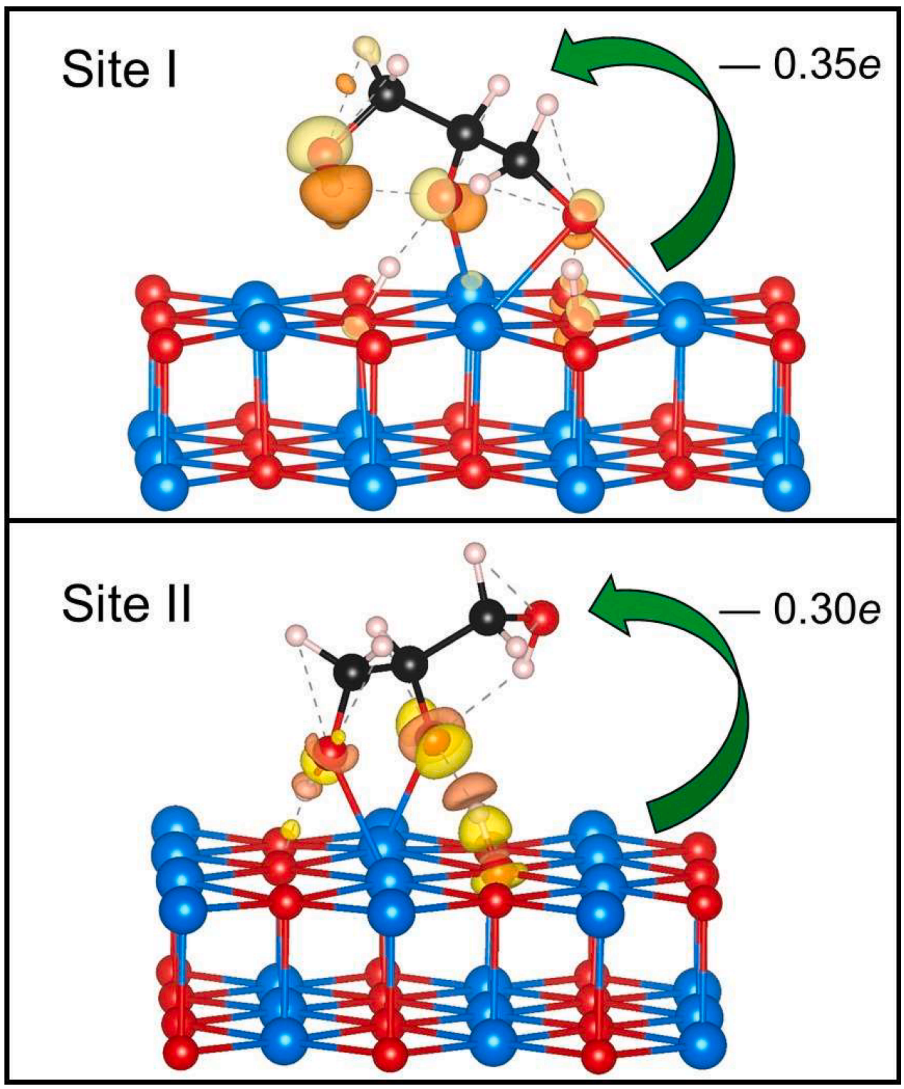

Fig. 6. Charge density difference for the two analyzed adsorption sites. The yellow colour indicates positive charge density while orange colour indicates negative charge.

$$\Delta\rho = \rho\ (\text{Glycerol}/\text{CaO}) - \rho(\text{CaO}) - \rho\ (\text{Glycerol})] \quad (2)$$

Where ρ (Glycerol/CaO) and ρ (CaO) are the charge density of the relaxed surfaces with and without adsorption respectively, and ρ (Glycerol) is the total charge density of the relaxed alcohol. Our results reveal a positive charge accumulation (orange regions) around the Ca and O species belonging to the surface in the neighborhood of the interaction site. Additionally, negative charge density can be observed around the Glycerol O atoms near the CaO surface, suggesting electron transfer from the surface to the adsorbate. These findings are consistent with the charge transfer values reported in Tables 5 and 6.

4. Conclusions

The adsorption of glycerol in CaO(001) has been studied by DFT calculations considering van der Waals corrections. Our work reveals a potential initial stage in the formation of an active glycerolate species, which binds to the surface while causing a substantial relaxation of the surface's bond order (up to 60%). During adsorption, surface $O_{glycerol}$–Ca bonds form, while the Ca–O bonds of the solid deteriorate. The BO of the OH bonds in glycerol decreases to the breaking point. Additionally, the H atom from glycerol interacts with surface oxygen, forming OH groups. The adsorption energy is −2.24 (−2.07), practically double that of methanol with the same surface area. The analysis of the electronic structure indicates stabilization after adsorption with shifts to lower energies with important participation of the s and p orbitals of glycerol. Considering the charge distribution, a transfer from the surface to the molecule of 0.35 (0.230)*e* is observed for the two most favorable studied sites.

CRediT authorship contribution statement

A.J.González Fá: Writing – original draft, Visualization, Validation, Software, Formal analysis, Data curation. **P. Bechthold:** Writing – review & editing, Writing – original draft, Validation, Supervision, Resources, Methodology, Investigation, Data curation. **A. Juan:** Writing – review & editing, Writing – original draft, Supervision, Project administration, Methodology, Investigation, Conceptualization. **J.M. Marchetti:** Writing – review & editing, Writing – original draft, Supervision, Software, Project administration, Investigation, Funding acquisition, Conceptualization.

Declaration of competing interest

The authors declare that they have no known competing financial interests or personal relationships that could have appeared to influence

the work reported in this paper.

Acknowledgments

The simulations were performed on resources provided by UNINETT Sigma2 the National Infrastructure for High Performance Computing and Data Storage in Norway. The work was funded by EU project UNPRECENDENTED HORIZON-MSCA-2021-SE-01-01 project number 101086363. AGF, PB, and AJ are members of CONICET, J.M.M acknowledge NMBU, Norway

Supplementary materials

Supplementary material associated with this article can be found, in the online version, at doi:10.1016/j.apsadv.2024.100657.

Data availability

Data will be made available on request.

References

[1] V.Banga Monika, V.V. Pathak, Biodiesel production from waste cooking oil : a comprehensive review on the application of heterogenous catalysts, Energy Nexus 10 (2010) 100209, https://doi.org/10.1016/j.nexus.2023.100209.
[2] B. Changmai, C. Vanlalveni, A.P. Ingle, R. Bhagatd, S.L. Rokhum, Widely used catalysts in biodiesel production : a review, RSC Adv. 10 (2020) 41625–41679, https://doi.org/10.1039/d0ra07931f.
[3] G. Knothe, Biodiesel and renewable diesel: a comparison, Prog. Energy Combust. Sci. 36 (2010) 364–373, https://doi.org/10.1016/j.pecs.2009.11.004.
[4] A.A. Abdul Raman, H.W. Tan, A. Buthiyappan, Two-step purification of glycerol as a value added by product from the biodiesel production process, Front. Chem. 7 (2019) 774, https://doi.org/10.3389/fchem.2019.00774.
[5] D.T. Oyekunle, M. Barasa, E.A. Gendy, S.K. Tiong, Heterogeneous catalytic transesterification for biodiesel production: feedstock properties, catalysts and process parameters, Process Saf. Environ. Prot. 177 (2023) 844–867, https://doi.org/10.1016/j.psep.2023.07.064.
[6] P. Maheshwari, M.B. Haider, M. Yusuf, J.J. Klemeš, A. Bokhari, M. Beg, A. Al-Othman, R. Kumar, A.K. Jaiswal, A review on latest trends in cleaner biodiesel production: role of feedstock, production methods, and catalysts, J. Clean. Prod. 355 (2022) 131588, https://doi.org/10.1016/j.jclepro.2022.131588.
[7] V.M.E. Melo, G.F. Ferreira, L.V. Fregolente, Sustainable catalysts for biodiesel production: the potential of CaO supported on sugarcane bagasse biochar, Renew. Sustain. Energy Rev. 189 (2024) 114042, https://doi.org/10.1016/j.rser.2023.114042.
[8] M.E. Kibar, L. Hilal, B.T. Çapa, B. Bahçıvanlar, B.Ben Abdeljelil, Assessment of Homogeneous and Heterogeneous Catalysts in Transesterification Reaction: a Mini Review, ChemBioEng Rev. 10 (2023) 412–422, https://doi.org/10.1002/cben.202200021.
[9] R. Garg, R. Sabouni, M. Ahmadipour, From waste to fuel: challenging aspects in sustainable biodiesel production from lignocellulosic biomass feedstocks and role of metal organic framework as innovative heterogeneous catalysts, Ind. Crops Prod. 206 (2023) 117554, https://doi.org/10.1016/j.indcrop.2023.117554.
[10] A.A. Refaat, Different techniques for the production of biodiesel from waste vegetable oil, Int. J. Environ. Sci. Tech. 7 (2010) 183–213, https://doi.org/10.1007/BF03326130.
[11] Z. Helwani, M.R. Othman, N. Aziz, W.J.N. Fernando, J. Kim, Technologies for production of biodiesel focusing on green catalytic techniques: a review, Fuel Process. Technol. 90 (2009) 1502–1514, https://doi.org/10.1016/j.fuproc.2009.07.016.
[12] M.R. Avhad, J.M. Marchetti, A review on recent advancement in catalytic materials for biodiesel production, Renew. Sustain. Energy Rev. 50 (2015) 696–718, https://doi.org/10.1016/j.rser.2015.05.038.
[13] B. Thangaraj, P.R. Solomon, B. Muniyandi, S. Ranganathan, L. Lin, Catalysis in biodiesel production - a review, Clean Energy 3 (2019) 2–23, https://doi.org/10.1093/ce/zky020.
[14] R. Ahmed, K. Huddersman, Review of biodiesel production by the esterification of wastewater containing fats oils and grease (FOGs), J. Ind. Eng. Chem. 110 (2022) 1–14, https://doi.org/10.1016/j.jiec.2022.02.045.
[15] P.L. Boey, G.P. Maniam, S.A. Hamid, Performance of calcium oxide as a heterogeneous catalyst in biodiesel production: a review, Chem. Eng. J. 168 (2011) 15–22, https://doi.org/10.1016/j.cej.2011.01.009.
[16] A.P.S. Chouhan, A.K. Sarma, Modern heterogeneous catalysts for biodiesel production: a comprehensive review, Renew. Sustain. Energy Rev. 15 (2011) 4378–4399, https://doi.org/10.1016/j.rser.2011.07.112.
[17] N.A. Zul, S. Ganesan, T.S. Hamidon, W. Da Oh, M.H. Hussin, A review on the utilization of calcium oxide as a base catalyst in biodiesel production, J. Environ. Chem. Eng. 9 (2021) 105741, https://doi.org/10.1016/j.jece.2021.105741.
[18] S.F. Basumatary, S. Brahma, M. Hoque, B.K. Das, M. Selvaraj, S. Brahma, S. Basumatary, Advances in CaO-based catalysts for sustainable biodiesel synthesis, Green Energy Resour. 1 (2023) 100032, https://doi.org/10.1016/j.gerr.2023.100032.
[19] Y. Fan, Y. Zhuo, L. Li, SeO_2 adsorption on CaO surface: DFT and experimental study on the adsorption of multiple SeO_2 molecules, Appl. Surf. Sci. 420 (2017) 465–471, https://doi.org/10.1016/j.apsusc.2017.04.233.
[20] V. Orazi, A. Juan, E.A. González, J.M. Marchetti, P.V. Jasen, DFT study of ethanol adsorption on CaO (001) surface, Appl. Surf. Sci. 500 (2020) 144254, https://doi.org/10.1016/j.apsusc.2019.144254.
[21] M. López Granados, A.C. Alba-Rubio, F. Vila, D. Martín Alonso, R. Mariscal, Surface chemical promotion of Ca oxide catalysts in biodiesel production reaction by the addition of monoglycerides, diglycerides and glycerol, J. Catal. 276 (2010) 229–236, https://doi.org/10.1016/j.jcat.2010.09.016.
[22] M. Kouzu, T. Kasuno, M. Tajika, S. Yamanaka, J. Hidaka, Active phase of calcium oxide used as solid base catalyst for transesterification of soybean oil with refluxing methanol, Appl. Catal. A Gen. 334 (2008) 357–365, https://doi.org/10.1016/j.apcata.2007.10.023.
[23] M. Kouzu, M. Tsunomori, S. Yamanaka, J. Hidaka, Solid base catalysis of calcium oxide for a reaction to convert vegetable oil into, Adv. Powder Technol. 21 (2010) 488–494, https://doi.org/10.1016/j.apt.2010.04.007.
[24] I. Malpartida, P. Maireles-Torres, C. Vereda, J.M. Rodríguez-Maroto, S. Halloumi, V. Lair, J. Thiel, F. Lacoste, Semi-continuous mechanochemical process for biodiesel production under heterogeneous catalysis using calcium diglyceroxide, Renew. Energy 159 (2020) 117–126, https://doi.org/10.1016/j.renene.2020.05.020.
[25] L. León-Reina, A. Cabeza, J. Rius, P. Maireles-Torres, A.C. Alba-Rubio, M. López Granados, Structural and surface study of calcium glyceroxide, an active phase for biodiesel production under heterogeneous catalysis, J. Catal. 300 (2013) 30–36, https://doi.org/10.1016/j.jcat.2012.12.016.
[26] M. Catarino, S. Martins, A. Soares Dias, M. Francisco, M. Costa Pereira, J. Gomes, Calcium diglyceroxide as a catalyst for biodiesel production, J. Environ. Chem. Eng. 7 (2019) 103099, https://doi.org/10.1016/j.jece.2019.103099.
[27] T. Li, X. Zhang, C. Zhang, R. Li, J. Liu, H. Zhang, P. Han, Z. Zheng, C. Fan, A Density Functional Theory Study on the Acid-Catalyzed Transesterification Mechanism for Biodiesel Production from Waste Cooking Oils, J. Am. Oil Chem. Soc. 96 (2019) 137–145, https://doi.org/10.1002/aocs.12178.
[28] M. Calatayud, Ethylene glycol interaction on alkaline earth oxides: a periodic DFT study, Catal. Today 152 (2010) 88–92, https://doi.org/10.1016/j.cattod.2009.08.011.
[29] P. Bechthold, V. Orazi, A. Juan, J.M. Marchetti, A first-principles study of formic acid adsorption on CaO (001), Appl. Surf. Sci. 583 (2022) 152296, https://doi.org/10.1016/j.apsusc.2021.152296.
[30] P. Bechthold, J. Juan, A. Juan, J.M. Marchetti, The adsorption of ethyl formate on CaO: a DFT study, J. Phys. Chem. Solids. 185 (2024) 111780, https://doi.org/10.1016/j.jpcs.2023.111780.
[31] P. Hohenberg, W. Kohn, Inhomogeneous electron gas, Phys. Rev. 136 (1964) B864–B871, https://doi.org/10.1103/PhysRev.136.B864.
[32] W. Kohn, L.J. Sham, Self-consistent equations including exchange and correlation effects, Phys. Rev. 140 (1965) A1133–AA113, https://doi.org/10.1103/PhysRev.140.A1133.
[33] G. Kresse, D. Joubert, From ultrasoft pseudopotentials to the projector augmented-wave method, Phys. Rev. B 59 (1999) 1758–1775, https://doi.org/10.1103/PhysRevB.59.1758.
[34] P.E. Blochl, Projector augmented-wave method, Phys. Rev. B 50 (1994) 17953–17979, https://doi.org/10.1103/PhysRevB.50.17953.
[35] G. Kresse, J. Furthmüller, Effective iterative schemes for ab initio total-energy calculations using a plane-wave basis set, Phys. Rev. B 54 (1996) 11169–11186, https://doi.org/10.1103/PhysRevB.54.11169.
[36] G. Kresse, J. Furthmüller, Efficiency of ab-initio total energy calculations for metals and semiconductors using a plane-wave basis set, Comput. Mater. Sci. 6 (1996) 15–50, https://doi.org/10.1016/0927-0256(96)00008-0.
[37] S. Grimme, J. Antony, S. Ehrlich, H. Krieg, A consistent and accurate ab initio parametrization of density functional dispersion correction (DFT-D) for the 94 elements H-Pu, J. Chem. Phys. 132 (15) (2010) 154104, https://doi.org/10.1063/1.3382344.
[38] H.J. Monkhorst, J.D. Pack, Special points for Brillouin-zone integrations, Phys. Rev. B 13 (12) (1976) 5188–5192, https://doi.org/10.1103/PhysRevB.13.5188.
[39] R. Hoffman, Solids and Surfaces: A Chemist's View of Bonding in Extended Structures, Wiley-VCH, US Dept of the Navy, 1988. http://www.dtic.mil/docs/citations/ADA196638.
[40] R.F.W. Bader, Atoms in molecules. Encycl. Comput. Chem, John Wiley &Sons, Ltd, Chichester, UK, 2002. http://doi.wiley.com/10.1002/0470845015.caa012.
[41] G. Henkelman, A. Arnaldsson, H. Jónsson, A fast and robust algorithm for Bader decomposition of charge density, Comput. Mater. Sci. 36 (3) (2006) 354–360, https://doi.org/10.1016/j.commatsci.2005.04.010.
[42] M. Yu, D.R. Trinkle, Accurate and efficient algorithm for Bader charge integration, J. Chem. Phys. 134 (6) (2011) 064111, https://doi.org/10.1063/1.3553716.
[43] T.A. Manz, N.G. Limas, Introducing DDEC6 atomic population analysis: part 1. Charge partitioning theory and methodology, RSC Adv. 6 (53) (2016) 47771–47801, https://doi.org/10.1039/C6RA04656H.
[44] N.G. Limas, T.A. Manz, Introducing DDEC6 atomic population analysis: part 2. Computed results for a wide range of periodic and nonperiodic materials, RSC Adv. 6 (51) (2016) 45727–45747, https://doi.org/10.1039/C6RA05507A.

[45] T.A. Manz, Introducing DDEC6 atomic population analysis: part 3. Comprehensive method to compute bond orders, RSC Adv. 7 (72) (2017) 45552–45581, https://doi.org/10.1039/c7ra07400j.
[46] N.G. Limas, T.A. Manz, Introducing DDEC6 atomic population analysis: part 4. Efficient parallel computation of net atomic charges, atomic spin moments, bond orders, and more, RSC Adv. 8 (5) (2018) 2678–2707, https://doi.org/10.1039/c7ra11829e.
[47] M. Calatayud, A.M. Ruppert, B.M. Weckhuysen, Theoretical study on the role of surface basicity and lewis acidity on the etherification of glycerol over alkaline earth metal oxides, Chem. - A Eur. J. 15 (2009) 10864–10870, https://doi.org/10.1002/chem.200900487.
[48] I. Lizana, J. Colmenares-Zerpa, G. Pecchi, R.J. Chimentão, E.J. Delgado, Conversion of glycerol to hydroxyacetone over $SrTiO_3$ -type perovskite: a DFT study, J. King Saud Univ. Sci. 33 (2021) 101597, https://doi.org/10.1016/j.jksus.2021.101597.
[49] I.M. Alliati, B.L. Irigoyen, A first-principles modeling of glycerol and ammonia interactions on the cation-deficient $VSbO_4$(1 1 0) surface, Catal. Today 254 (2015) 53–61, https://doi.org/10.1016/j.cattod.2014.12.025.
[50] C. Di Valentin, D. Fittipaldi, Hole Scavenging by Organic Adsorbates on the TiO_2 Surface: a DFT Model Study, J. Phys. Chem. Lett. 4 (2013) 1901–1906, https://doi.org/10.1021/jz400624w.
[51] C. Rohmann, H. Idriss, A computational study of the interaction of oxygenates with the surface of rutile TiO_2(110). Structural and electronic trends, J. Phys. Condens. Matter. 34 (2022) 154002, https://doi.org/10.1088/1361-648X/ac4d5b.
[52] S.Niu Z.Li, K. Han, Y. Li, Y. Wang, C. Lu, S. Cheng, Investigation into influences of methanol pre-adsorption on CaO(100) surface in transesterification for biodiesel production with molecular simulation, Appl. Catal. A-Gen. 609 (2021) 117908, https://doi.org/10.1016/j.apcata.2020.117908.
[53] Z. Li, S. Niu, G. Zhao, Y.Li K.Han, C. Lu, S. Cheng, Molecular simulation study of strontium doping on the adsorption of methanol on CaO(100) surface, J. Fuel Chem. Technol. 48 (2) (2020) 172–178, https://doi.org/10.1016/S1872-5813(20)30008-6.
[54] A. Esipovich, A. Rogozhin, S. Danov, A. Belousov, E. Kanakov, The structure, properties and transesterification catalytic activities of the calcium glyceroxide, Chem. Eng. J. 339 (2018) 303–316, https://doi.org/10.1016/j.cej.2018.01.142.